Margarit Benavent, VJ.; Díaz-Rey, MDR.; Navarro Villalba, MT.; Martínez, C.; Corma Canós, A. (2018). Direct Synthesis of Nano-Ferrierite along the 10-Ring-Channel Direction Boosts Their Catalytic Behavior. Angewandte Chemie International Edition. 57(13):3459-3463. https://doi.org/10.1002/anie.201711418

Direct synthesis of nano-ferrierite along the 10-ring channels direction boost the catalytic behavior

Vicente J. Margarit, M. Rocío Díaz-Rey, M. Teresa Navarro, Cristina Martínez*, Avelino Corma*

Abstract: Ferrierite zeolites with nanosized crystals and external surface areas higher than 250 $m^2 \cdot g^{-1}$ have been prepared at relatively low synthesis temperature (120ºC) by means of the collaborative effect of two Organic Structure Directing Agents (OSDA). In this way, hierarchical porosity is achieved without the use of post-synthesis treatments that usually involve leaching of T atoms and solid loss. Adjusting the synthesis conditions it is possible to decrease the crystallite size in the directions of the 8- and 10-ring channels, [010] and [001] respectively, increasing the number of pores accessible and reducing their average pore length to 10-30 nm. The small crystal size of the nano-ferrierites results in an improved accessibility of reactants to the catalytic active centers and enhanced product diffusion, leading to higher conversion and selectivity with lower deactivation rates for the oligomerization of 1-pentene into longer-chain olefins.

Zeolites are microporous silico-aluminates with crystalline structures presenting well defined channels and cavities of molecular dimensions,[1] widely employed as adsorbents, ion exchangers and for gas separation or refining, petrochemical and environmental catalytic applications [2] due to their molecular sieve and shape selectivity effects [3]. Nevertheless, based on confinement effects, a new concept and methodology for the “Ab initio" synthesis of zeolites for preestablished catalytic reactions has been reported very recently [4]. In processes dealing with bulky molecules, their microporous structure may impose diffusional problems and underuse of the overall micropore volume, directly affecting activity, selectivity and deactivation rate. Among the different approaches proposed to increase the accessibility to the zeolites active sites [5], the generation of inter-crystalline mesoporosity by reducing the crystallite size from the micro- to the nanoscale [5d, 6] has been thoroughly explored in the last years.

Ferrierite [FER] is a zeolite with a bidirectional microporous structure formed by interconnected medium (10-ring, 4.2 x 5.4 Å) and small (8-ring, 3.5 x 4.8 Å) pores. Along the 8-ring channels a cavity is formed, accessible only through 8-ring windows, and known as the FER cage [7] . This zeolite, highly stable towards thermal, hydrothermal and chemical treatments, has been applied as catalyst in different processes, such as isomerization of n-butenes [8] and others [9].

Although highly selective, the topology and pore dimensions of ferrierite limits the reaction to the active sites closer to the crystal surface and results in fast deactivation due to pore blocking with coke precursors. One possible solution would be to decrease the diffusional path lengths. Thus, a delaminated FER, ITQ-6, was obtained by delamination of a layered precursor (PREFER) [10], following a procedure similar to the one used for preparing zeolite ITQ-2 [6]. When efficiently delaminated, ITQ-6 is highly active for the conversion of bulky reactants [10b] due to its high external surface area. However, its reduced micropore volume results in decreased shape selectivity and confinement effects. Mesoporosity generation in ferrierite crystallites by post-synthesis desilication treatments has also been attempted [11], but this procedure is less efficient than in other zeolites due to its high chemical stability [11a, 12].

A different approach is the direct synthesis of nanocrystalline ferrierite with different morphologies (see **Scheme 1**), and nanocrystals (40-60 nm) [13] or nanoneedles (10 x 100 nm) [14] have been reported. Although these zeolites can be considered as nanosized, decreasing crystal size from 40 to 10-15 nm can have an enormous effect on initial activity, selectivity and catalyst life [15]. Regarding the nanoneedles, as they grow along the direction of the 10-ring channels, the diffusion path lengths are not reduced in this case. Other groups describe the synthesis of ferrierite nanocrystal aggregates [16] or the crystallization of FER nanosheet assemblies[17], but none of the final solids combine high external

surface areas with acceptable micropore volumes. Thus, the most interesting and challenging objective, i.e., to obtain very small nanocrystals (<15 nm) along the [001] direction of the 10-ring channels, maintaining a well-preserved microporous structure, has not yet been achieved, as far as we know.

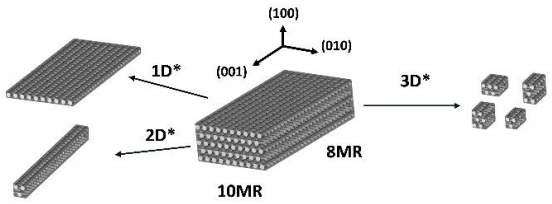

Scheme 1. Representation of crystal size reduction in (100) (1D), in (100) and (010) (2D) and (100), (010) and (001) (3D) to ferrierite layers, needles and nanocrystals, respectively.

For that purpose, we propose in this work the cooperative use of piperidine and a modified surfactant for the synthesis of ferrierite nanozeolites under hydrothermal conditions (see **Table S1**). Varying the synthesis time (7-17 days) and temperature (120-150ºC) nanoferrierites were obtained with the smallest crystal size in the (001) and (010) directions reported so far. Although the use of modified surfactants as single OSDAs has successfully led to the one pot synthesis of layered MWW [18], MFI and MOR [19], and nanosized BEA [20] zeolites, this strategy involves high costs related to the OSDA preparation, which requires multiple steps and large excess of reagents. Thus, a cheaper option is to introduce a simpler modified surfactant in combination with the classical OSDA [21], which is the approach followed in this work.

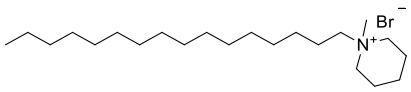

Figure 1. Modified Surfactant C_{16}MPip.

Piperidine (Pip) is known to direct the synthesis towards the crystallization of ferrierite [22]. Moreover, we have added cetylmethylpiperidinium bromide, C_{16}MPip (see **Figure 1**) to the synthesis media, a surfactant easily obtained by alkylation of N-methylpyperidine with 1-bromohexadecane (see Supporting Information for more details). Piperidine is expected to initiate the crystallization of the FER structure, and in a similar way, the piperidine-derived head of the surfactant should fit into the microporous channel system, whereas the long carbon chain should limit crystal growth. Both OSDAs, piperidine and the modified surfactant, were stable within the zeolite structure under the synthesis conditions (see **Figure S1 and S2**).

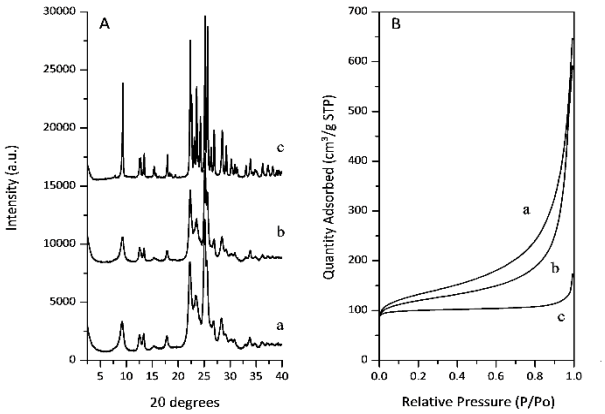

Figure 2. XRD patterns of as synthesized ferrierites (A) and nitrogen adsorption isotherms (B) of the acid ferrieriets. N-FER(15) synthesized at 120ºC (a), 150ºC (b) and R-FER (c).

Ferrierite is crystallized in all cases as a single phase (see **Figures 2A, S3A** and **S4A**), and the structure is maintained after obtaining the acid form of the zeolite (see **Figure S3B** and **S4B**). When compared to a reference zeolite synthesized at 150ºC using piperidine as a single OSDA (R-FER), the diffraction peaks of the nano-ferrierites are significantly broader and less intense, suggesting a notably smaller crystal size.

The shape of the nitrogen adsorption isotherms obtained for the N-FER and the conventional ferrierite evidence their different textural properties (see **Figures 2B** and **S5**). R-FER showed a type I isotherm, typical of microporous materials. This zeolite, with a total pore volume of 0.27 $cm^3 \cdot g^{-1}$ and a micropore volume of 0.149 $cm^3 \cdot g^{-1}$, has a very low contribution of the external surface area (17 $m^2 \cdot g^{-1}$) to the total BET value (320 $m^2 \cdot g^{-1}$) (see **Table S2**). In the case of the N-FER zeolites, the isotherms have a type IV shape, typical of materials presenting mesoporosity. The external surface areas increase to 157 and 262 $m^2 \cdot g^{-1}$ for the N-FER synthesized with Si/Al molar ratios of 15 at 150ºC and 120ºC, respectively. In both cases the total pore volume increases up to ≈0.9-1.0 $cm^3 \cdot g^{-1}$ (see **Table S2),** while preserving most of the micropore volume (0.09-0.12 $cm^3 \cdot g^{-1}$). Still, the argon isotherms in the low-pressure region show a small but increasing reduction of the volume adsorbed when decreasing crystal size (see **Figures S6**).

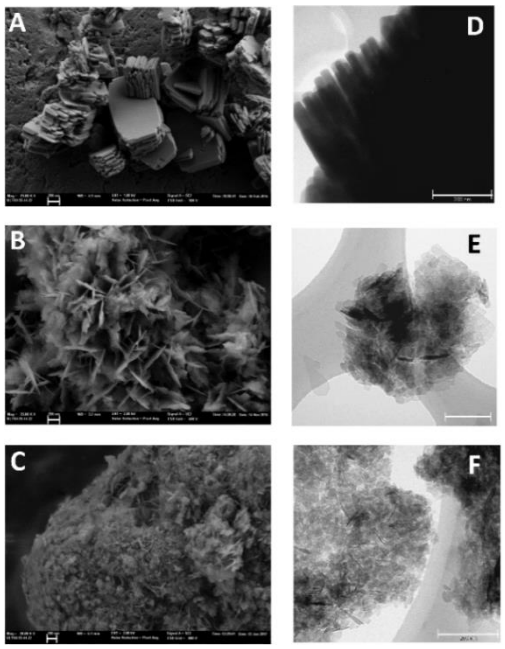

Figure 3. FESEM (A-C) and TEM (D-F) images corresponding to zeolites R-FER(15) (A,D), N-FER(15)-150 (B,E) and N-FER(15)-120 (C,F). Scale bar corresponds to 200 nm in all images.

The much smaller particle size of N-FER as compared to the reference ferrierite is confirmed by electron microscopy. The FESEM images (see **Figure 3A)** reveal the plate-like shape of the R-FER crystals with a preferential crystal growth in the *b-c* plane [23]. In the case of the N-FER two different morphologies are observed (see **Figures 3B-C and Figures S7A-E**): nanocrystals, isotropic in shape, where the crystal size in the *b-c* plane is largely decreased as compared to the plate-like morphology, and layered leave-shaped crystals (see also Scheme 1).

When lowering the synthesis temperature there is a clear crystal size reduction for both type of crystallites, and an increased proportion of the nanocrystals. This has been related to differences in activation energy for the stages of nucleation and crystal growth during the synthesis of the zeolite [1, 24]. Thus, sample N-FER(15)-120 mainly crystallizes as nanocrystals with sizes in the range of 10-20 nm (see HRTEM images in **Figure S8**). Structure-morphology relations

can be clearly observed in **Figure 4.** In this HRTEM image three different crystals are clearly visualized, a small isotropic nanocrystal (A), facing the (001) direction, and two layer-shaped crystals, one exposing the (010) orientation (B), and the other showing the (100) orientation but tilted 45º over the (010) axis (C). Crystallite intergrowth or twinning, as those described for MFI[25], have not been observed.

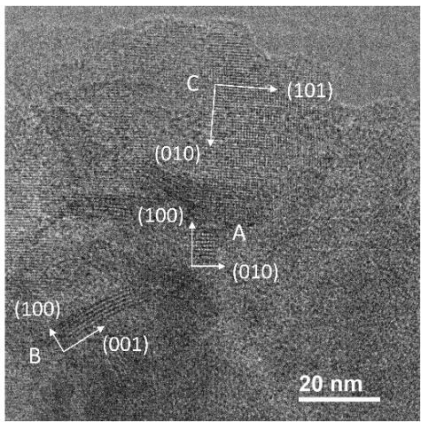

Figure 4. HRTEM image of N-FER(15)-150.

The Si/Al ratios of the calcined samples are 9 and 10 to 12 for the R-FER and the N-FER(15) zeolites, respectively (see **Table S2)**. This aluminum exhibits a tetrahedral coordination in the as-made material (see the ^{27}Al-MAS-NMR spectra in **Figure S9**) and a good thermal stability, with 85% of the trivalent element remaining in framework positions in the final acid zeolites. It should be remarked that the smaller crystal size of the N-FER as compared to the R-FER does not result in a larger dealumination during the zeolite calcination process. This framework Al^{3+} confers the zeolite its Brønsted acidity (see **Figure S10**).

In microcrystalline ferrierites an important fraction of the Brønsted acid sites is not accessible to most of the reactants, as part of the protons may be pointing into the 8-ring channels or into the FER cages, being only accessible through 8-ring windows [10b, 25-26]. Indeed, only 40% of the total sites in R-FER are accessible to pyridine (see **Figure S10** and **Table S3**), but more than 55% of the sites are accessible in the N-FER(15) samples.

The remarkable textural properties of the N-FER zeolites, combining well preserved micropore volumes (≈ 0.09 $cm^3 \cdot g^{-1}$) and external surface areas above 260 $m^2 \cdot g^{-1}$, the increased exposure of 10-ring pore mouths and the reduced length of these 10-ring channels, should result in an improved catalytic behavior when used as acid catalysts. Thus, N-FER in their acid form have been used to catalyze the oligomerization of 1-pentene to liquid fuels under industrially relevant liquid phase conditions, at 200°C and 4.0 MPa and space velocity (WHSV) of 3 to 50 h^{-1} in a down-flow fixed bed reactor (see Supporting Information for details). Oligomerization of light alkenes to liquid fuels is a process of increasing applied interest [2b, 27] as it enables the conversion of olefins in the C3 to C6 range present in orphan or low value industrial streams into clean liquid fuels such as gasoline, jet fuel or diesel [28]. Ferrierites have been described as active for oligomerization of pentenes [29] and 1-butene [30], highly selective to dimers and trimers, respectively. However, selectivity to the most interesting diesel range oligomers is low and the catalysts rapidly deactivate due to pore blocking by deposition of heavier hydrocarbons inside the micropores. Still, the synthesis of the N-FER with very short 10-ring channels may offer ferrierite a new opportunity as olefin oligomerization catalyst.

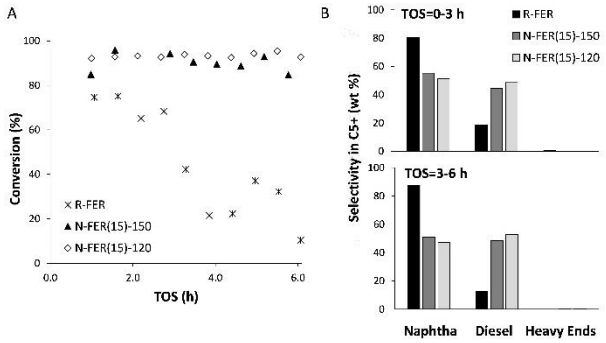

Figure 5. (A) 1-Pentene conversion vs. TOS and (B) selectivity within the C_{5+} liquid fraction for ferrierite zeolites at WHSV=8 h^{-1}, T=200°C, P = 4.0 MPa, 60% mol olefin in the feed.

When comparing the activity of the reference R-FER and the nano-ferrierite zeolites with Si/Al ratios of 15 synthesized at 150ºC and 120°C at WHSV=8 h^{-1} (see **Figure 5A)**, the initial olefin conversion is increased from 80% to values above 90% obtained with the N-FER(15) zeolites. However, the most remarkable result is the improvement of catalyst life. Working at this very high WHSV to study the deactivation behavior at short times on stream, the N-FER zeolites maintain the initial activity for 6 hours, whereas the conventional ferrierite gives olefin conversions below 50% after 3 h of reaction. When comparing with the sample with less Al, N-FER(30), the latter is slightly less active than the N-FER(15) samples (see **Figure S11**), in good agreement with its lower Brønsted site density (see **Table S3**), but deactivation rate is comparable. It has to be remarked that working at WHSV=3.3 h^{-1}, still in the upper limit of that relevant for industrial operation, catalyst N-FER(15)-120 presents olefin conversion above 95% after 24 h bench scale experiment (see **Figure S12**).

Regarding product selectivity, **Figure 5B** shows that the smaller crystal size along the 10-ring channels of the nanocrystalline ferrierites favors the formation of oligomers in the diesel range (mainly C15 trimers).

When increasing the operation severity to WHSV = 15, 25 and 50 h^{-1}, the differences among the nano-ferrierites become larger (see **Figure S13 and Figure S14**) and initial activity and catalyst life are in direct correlation with the crystal size of the nano-zeolites (N-FER(15)-150<N-FER(15)-125<N-FER(15)-120). It is not until space velocity is increased to values as high as 50 h^{-1} that we see a clear activity loss with TOS for the N-FER(15) zeolites. Notice that R-FER presented an initial olefin conversion below 20%, and no pentene conversion after 3 hours on stream already at a space velocity of 25 h^{-1}.

Summarizing, we have presented a simple procedure to synthesize nanosized ferrierites in the presence of two cooperative OSDAs, piperidine and C_{16}MPip, with good solid yields. The nano-ferrierites present crystallite dimensions in the *bc* plane as low as 10x10 nm, corresponding to 13 unit cells along the direction of the 10-ring channels, and Si/Al ratios in the range of 8 to 20. These N-FER, with external surface areas as high as 262 $m^2 \cdot g^{-1}$, mesopore and total pore volumes of 0.43 and 1.00 $cm^3 \cdot g^{-1}$, respectively, present increased accessibility to the Brønsted acid sites, higher activity and diesel selectivity, and longer catalyst life than a microsized reference for the liquid phase oligomerization of 1-pentene. The outstanding catalytic behavior observed is mainly due to the reduced crystallite size along the (001) direction, reducing the diffusional path length of the molecules along the 10-ring channels.

Experimental Section

Details on the synthesis of the ferrierite zeolites and of the ODSA C_{16}MPip can be found in the Supporting Information. Liquid phase oligomerization of 1-pentene was performed in a down-flow stainless-steel fixed-bed reactor at 200°C, 4.0 MPa, and WHSV in the range of 3 to 50 h^{-1}. A detailed description is given in the Supporting Information.

Acknowledgements

This work has been supported by the European Union through the European Research Council (ERC-AdG-2014-671093, SynCatMatch) the Spanish government through the “Severo Ochoa Program” (SEV-2016-0683) and CTQ2015-70126-R, and by the Fundación Ramón Areces through a research project within the “Life and Materials Sciences” program. M.R.D-R. acknowledges “La Caixa - Severo Ochoa” International PhD Fellowships (call 2015). The Electron Microscopy Service of the Universitat Politècnica de València is acknowledged for its help in sample characterization. The authors thank Dr. Manuel Moliner for helpful discussions.

Keywords: Nano-zeolite, ferrierite [FER], modified surfactant as OSDA, 1-pentene oligomerization, catalyst lifetime.

[1] C. S. Cundy, P. A. Cox, Microporous Mesoporous Mater. 2005, 82, 1.

[2] a) M. E. Davis, Nature 2002, 417, 813-821; b) C. Martínez, A. Corma, Coordination Chemistry Reviews 2011, 255, 1558-1580; c) M. Tsapatsis, Science 2011, 334, 767-768.

[3] a) S. Teketel, W. Skistad, S. Benard, U. Olsbye, K. P. Lillerud, P. Beato, S. Svelle, ACS Catalysis 2012, 2, 26-37; b) B. Smit, T. L. M. Maesen, Nature 2008, 451, 671-678; c) T. F. Degnan Jr, Journal of Catalysis 2003, 216, 32-46.

[4] E. M. Gallego, M. T. Portilla, C. Paris, A. León-Escamilla, M. Boronat, M. Moliner, A. Corma, Science 2017, 355, 1051-1054.

[5] a) J. Jiang, J. Yu, A. Corma, Angewandte Chemie International Edition 2010, 49, 3120-3145; b)J. Perez-Ramirez, C. H. Christensen, K. Egeblad, C. H. Christensen, J. C. Groen, Chem. Soc. Rev. 2008, 37, 2530-2542; c) V. Valtchev, G. Majano, S. Mintova, J. Perez-Ramirez, Chemical Society Reviews 2013, 42, 263-290; d) S. Mintova, M. Jaber, V. Valtchev, Chem. Soc. Rev. 2015, 44, 7207-7233; e)A. H. Janssen, I. Schmidt, C. J. H. Jacobsen, A. J. Koster, K. P. de Jong, Microporous and Mesoporous Materials 2003, 65, 59-75.

[6] A. Corma, V. Fornes, S. B. Pergher, T. L. M. Maesen, J. G. Buglass, Nature 1998, 396, 353-356.

[7] a) C. Baerlocher, L. B. McCusker, D. H. Olson, in Atlas of Zeolite Framework Types (Sixth Edition), Elsevier Science B.V., Amsterdam, 2007, pp. 142-143; b) M. Moliner, C. Martínez, A. Corma Angewandte Chemie International Edition 2015, 54, 3560-3579.

[8] W. Vermeiren, J.-P. Gilson, Top. Catal. 2009, 52, 31.

[9] a) P. Cheung, A. Bhan, G. J. Sunley, E. Iglesia, Angewandte Chemie International Edition 2006, 45, 1617-1620; b) Y. Román-Leshkov, M. Moliner, M. E. Davis, The Journal of Physical Chemistry C 2011, 115, 1096-1102; c) I. Melian-Cabrera, S. Espinosa, F. J. Garcia-Montelongo, F. Kapteijn, J. A. Moulijn, Chem. Commun. (Cambridge, U. K.) 2005, 1525-1527; d) J. A. Martens, A. Cauvel, A. Francis, C. Hermans, F. Jayat, M. Remy, M. Keung, J. Lievens, P. A. Jacobs, Angew. Chem., Int. Ed. 1998, 37, 1901-1903; e) T. Nanba, A. Obuchi, H. Izumi, Y. Sugiura, J. Xu, J. Uchisawa, S. Kushiyama, Chem. Commun. (Cambridge) 2001, 173-174; f) S. C. C. Wiedemann, J. A. Stewart, F. Soulimani, T. van Bergen-Brenkman, S. Langelaar, B. Wels, P. de Peinder, P. C. A. Bruijnincx, B. M. Weckhuysen, J. Catal. 2014, 316, 24-35; g) H. L. Ngo, A. Nunez, W. Lin, T. A. Foglia, Eur. J. Lipid Sci. Technol. 2007, 109, 214-224; h) A. Corma, P. J. Miguel, V. Blay, Catalysis Science & Technology 2017.

[10] a) L. A. Chica, C. A. Corma, S. V. Fornes, M. U. Diaz, WO2000024673 A1, 2000; b) A. Corma, U. Diaz, M. E. Domine, V. Fornes, Angewandte Chemie, International Edition 2000, 39, 1499-1501.

[11] a) A. Bonilla, D. Baudouin, J. Pérez-Ramírez, Journal of Catalysis 2009, 265, 170-180; b) D. Verboekend, R. Caicedo-Realpe, A. Bonilla, M. Santiago, J. Perez-Ramirez, Chem. Mater., ACS ASAP.

[12] a) J. C. Groen, L. A. A. Peffer, J. A. Moulijn, R. Pérez, amp, x, J. rez, Microporous and Mesoporous Materials 2004, 69, 29-34; b) K. Brylewska, K. A. Tarach, W. Mozgawa, Z. Olejniczak, U. Filek, K. Góra-Marek, Journal of Molecular Structure 2016, 1126, 147-153.

[13] W. Chu, X. Li, X. Zhu, S. Xie, C. Guo, S. Liu, F. Chen, L. Xu, Microporous and Mesoporous Materials 2017, 240, 189-196.

[14] Y. Lee, M. B. Park, P. S. Kim, A. Vicente, C. Fernandez, I.-S. Nam, S. B. Hong, ACS Catalysis 2013, 3, 617-621.

[15] a) R. Martinez-Franco, C. Paris, M. E. Martinez-Armero, C. Martinez, M. Moliner, A. Corma, Chemical Science 2016, 7, 102-108; b) M. R. Diaz Rey, C. Paris, R. Martinez-Franco, M. Moliner, C. Martinez, A. Corma, ACS Catalysis 2017.

[16] T. Xue, H. Liu, Y. M. Wang, RSC Advances 2015, 5, 12131-12138.

[17] P. Wuamprakhon, C. Wattanakit, C. Warakulwit, T. Yutthalekha, W. Wannapakdee, S. Ittisanronnachai, J. Limtrakul, Microporous and Mesoporous Materials 2016, 219, 1-9.

[18] H. Y. Luo, V. K. Michaelis, S. Hodges, R. G. Griffin, Y. Roman-Leshkov, Chemical Science 2015.

[19] a) M. Choi, K. Na, J. Kim, Y. Sakamoto, O. Terasaki, R. Ryoo, Nature 2009, 461, 246-249; b) C. Jo, J. Jung, H. S. Shin, J. Kim, R. Ryoo, Angewandte Chemie International Edition 2013, 52, 10014-10017.

[20] M. Choi, K. Na, R. Ryoo, Chemical Communications 2009, 2845-2847.

[21] X. Zhu, R. Rohling, G. Filonenko, B. Mezari, J. P. Hofmann, S. Asahina, E. J. M. Hensen, Chem. Commun. 2014, 50, 14658-14661.

[22] G. Pál-Borbély, H. K. Beyer, Y. Kiyozumi, F. Mizukami, Microporous and Mesoporous Materials 1998, 22, 57-68.

[23] V. R. R. Marthala, M. Hunger, F. Kettner, H. Krautscheid, C. Chmelik, J. Kärger, J. Weitkamp, Chemistry of Materials 2011, 23, 2521-2528.

[24] L. Tosheva, V. P. Valtchev, Chemistry of Materials 2005, 17, 2494-2513.

[25] X. Zhang, D. Liu, D. Xu, S. Asahina, K. A. Cychosz, K. V. Agrawal, W. Y. Al, A. Bhan, H. S. Al, O. Terasaki, M. Thommes, M. Tsapatsis, Science 2012, 336, 1684-1687.

[26] a) M. A. Asensi, A. Martinez, Appl. Catal., A 1999, 183, 155-165; b) A. B. Pinar, C. Márquez-Álvarez, M. Grande-Casas, J. Pérez-Pariente, Journal of Catalysis 2009, 263, 258-265.

[27] a) S. Peratello, M. Molinari, G. Bellussi, C. Perego, Catal. Today 1999, 52, 271-277; b) O. Muraza, Industrial & Engineering Chemistry Research 2015, 54, 781-789; c) A. Corma, C. Martinez, E. Doskocil, J. Catal. 2013, 300, 183-196; d) C. Martínez, E. Doskocil, A. Corma, Topics in Catalysis 2014, 57, 668-682.

[28] a) A. Corma, E. Corresa, Y. Mathieu, L. Sauvanaud, S. Al-Bogami, M. S. Al-Ghrami, A. Bourane, Catalysis Science & Technology 2017, 7, 12-46; b) A. de Klerk, P. M. Maitlis, in Greener Fischer-Tropsch Processes for Fuels and Feedstocks, Wiley-VCH, 2013, pp. 81-105; c) Z. Y. Zakaria, J. Linnekoski, N. A. S. Amin, Chemical Engineering Journal 2012, 207–208, 803-813; d) Q. Wang, X. Chen, A. N. Jha, H. Rogers, Renewable and Sustainable Energy Reviews 2014, 30, 1-28.

[29] A. Kulkarni, A. Kumar, A. S. Goldman, F. E. Celik, Catalysis Communications 2016, 75, 98-102.

[30] Y. T. Kim, J. P. Chada, Z. Xu, Y. J. Pagan-Torres, D. C. Rosenfeld, W. L. Winniford, E. Schmidt, G. W. Huber, Journal of Catalysis 2015, 323, 33-44.